Published in final edited form as:
Ann Biomed Eng. 2014 January ; 42(1): 149–161. doi:10.1007/s10439-013-0894-3.

Heterogeneous susceptibility of valve endothelial cells to mesenchymal transformation in response to TNFα

Emily J. Farrar and **Jonathan T. Butcher**
Department of Biomedical Engineering, Cornell University, Ithaca, NY

Abstract

Lack of understanding of the early mechanisms of aortic valve stenosis and calcification hinders the development of diagnostic and therapeutic intervention strategies. Inflammation is a known component of early aortic valve disease (AVD) and can induce mesenchymal transformation in a subset of aortic valve endothelial cells. Here we present a three-dimensional culture system that allows transforming and non-transforming cells to be independently isolated and analyzed. We have used the system to identify and characterize the dynamic invasion and phenotypic transition of two distinct subsets of endothelial cells: those that invade and transform under TNFα treatment, and those that resist mesenchymal transformation and remain endothelial. We determine that non-transformed cells maintain control levels of endothelial genes VE-cadherin and eNOS, while transformed cells lose these endothelial characteristics and upregulate α-smooth muscle actin. Both subsets of cells have an inflammatory phenotype marked by increased ICAM-1, but transformed cells have increased MMP-9, Notch1, TGF-β, and BMP4, while non-transformed cells do not. Transformed cells also have distinct effects on alignment of collagen fibers as they invade the hydrogel system, which is not found in control endothelial or interstitial valve cells. Understanding the role of transforming and non-transforming endothelial cells in valve disease will provide an important pathological link between early inflammation and later stages of disease. Discovery of the molecular signature of transformation-resistant endothelial cells could inform development of treatment strategies that promote survival of the valve endothelium.

Keywords

aortic valve; calcification; EMT; invasion; inflammation; membrane; valve interstitial cells

Introduction

Aortic valve disease (AVD) affects 2.8% of Americans over 75 years of age. Approximately 40% of severe cases undergo cardiothoracic surgery[14] due to the lack of effective pharmaceutical treatments for AVD. Without surgical intervention, the majority of affected patients will die within one year of diagnosis[29]. Inflammation is a hallmark of early aortic valve disease[18] and new molecular imaging techniques have identified endothelial activation and damage to be a key early response[1]. However, limited understanding of the role of inflamed endothelial cells in AVD prohibits development of clinically useful strategies targeting valve endothelial pathobiology.

Address for correspondence: Jonathan T. Butcher, PhD, Associate Professor, Department of Biomedical Engineering, 304 Weill Hall, Cornell University, Ithaca, NY 14853. Phone: 607-255-3575, Fax: 607-255-7330, jtb47@cornell.edu.

Conflicts of Interest: None.

Recent studies suggest that valve endothelial function is a key regulator of early AVD via recruitment of immune cells[14], dysregulation of protective nitric oxide signaling[27], phenotypic plasticity[32], and through expression of pro-calcific proteins[28]. We recently showed that inflammatory cytokine TNFα drives an endothelial to mesenchymal transition (EndMT) in a subset (5–10%) of adult valve endothelial cells (VEC)[24]. Adult VEC EndMT also occurs in response to pathological levels of mechanical strain[3], elevated TGF-β signaling[26], or activation of cell-signaling ligand Notch1[33]. These studies used clonal isolations of valve endothelial cells and found, similar to inflammatory-EndMT, that mesenchymal transformation occurred only in a fraction of VEC. This subset of VEC that is uniquely able to transform under EndMT stimuli may have important roles in later AVD. A subset of VEC clonally isolated from MV can undergo EndMT and exhibits the capacity for osteogenic differentiation, suggesting their potentially unique participation in advanced mitral valve disease[32,4]. It is unknown how EndMT-VEC in the aortic valve participate in advanced AVD. In addition, the subset of VEC that do not transform may possess unique phenotypic signatures which promote resistance to mesenchymal transformation and potentially an ability to protect against disruption of the protective endothelial layer. These intriguing questions have not been examined due to the difficulty of separating transforming from non-transforming cells during EndMT. Studies are needed which are able to characterize transforming and non-transforming VEC in a controlled manner, elucidating the three-dimensional and time-dependent EndMT response of VEC to pathological conditions.

Here we have designed a system consisting of a porcine aortic valve endothelial cells cultured on a porous membrane combined with a collagen hydrogel. Endothelial cells treated with EndMT stimuli can invade, interact with a collagen gel matrix, and be separately isolated and studied from non-transformed endothelial cells. Aortic valve endothelial cells can maintain an endothelial phenotype on the membrane for up to six days, or undergo a full mesenchymal transformation by invading the underlying matrix. We used the system to characterize time-dependent dynamics of the TNFα-EndMT process, involving distinct stages of endothelial or myofibroblastic protein expression. We identified a unique sub-population of non-transforming cells that maintained endothelial characteristics under TNFα, suggesting resistance to EndMT. We also isolated a subset of transforming endothelial cells, in which we quantified the expression of genes related to aortic valve disease, including MMP9, TGF-β1, Notch1, and BMP4. Finally, we examined the effects of the transforming cells on their surrounding collagen matrix, as an initial investigation of the ability of these cells to contribute to valvular matrix remodeling. These results are an important step forward in characterizing valvular endothelial cells transformed by inflammatory EndMT and understanding their role in the progression of aortic valve disease. Furthermore, the ability to segregate and study a population of non-transforming VEC which are resistant to inflammatory EndMT establishes a foundation for identifying molecular mechanisms which may provide protection against mesenchymal transformation.

Methods and Materials

Cell isolation and culture

Porcine aortic valve endothelial cells (PAVEC) and porcine valve interstitial cells (PAVIC) were isolated as demonstrated previously[16] from valves donated by Shirk Meats of Dundee, NY. PAVEC were grown in flasks coated with 50 μg/mL rat-tail collagen I (BD Biosciences, San Jose, CA) at 37°C and 5% CO2 in DMEM supplemented with 10% FBS (Invitrogen, Grand Island, NY), 1% penicillin-streptomycin (Invitrogen, Grand Island, NY), and 50U/mL heparin (Sigma-Aldrich, St Louis, MO). Cells were passaged 1:3 at confluency using 0.25% Trypsin-EDTA (Invitrogen,) and media was changed every 48 hours. PAVIC were cultured identically, but without collagen flask coating or heparin in the culture media. Purity of endothelial population was monitored via quantitative real-time PCR, western blot,

and immunofluorescent assessment. Only cultures with consistent CD31 and VE-cadherin expression, cobblestone morphology, and non-detectable αSMA expression were used. αSMA levels were measured via real-time PCR (> 37 cycle threshold), western blot, and immunofluorescence. PAVEC and PAVIC cultures were used between passage four and six.

3-D culture system

Tissue-culture treated, sterile, polycarbonate membrane inserts (Corning, Inc., Corning, NY) were obtained in three and eight micron pore sizes and machined to a depth of 0.5mm. Membranes were coated in collagen I, 50 μg/mL (BD Biosciences, San Jose, CA) and filled with collagen gel composed of 10% FBS (Gemini Biosciences, West Sacramento, CA), 1× Dulbecco's modified eagle medium (D-MEM, Invitrogen, Grand Island, NY), and 2 mg/mL collagen type I (BD Biosciences, San Jose, CA), adjusted to a pH of 7.2. After one hour incubation at 37°C, PAVEC were seeded at 100,000 cells/cm^2 and allowed to adhere overnight. Membrane system was then carefully submerged in D-MEM+10% FBS and 0.5 g/L heparin (Invitrogen, Grand Island, NY), which served as the control media for all experiments. For experiments, 30 ng/mL TNFα (Sigma Aldrich, St Louis, MO) was added to control media. Membrane system was completely submerged in either control or +TNFα media for two to six days (Figure 1). PAVIC gels were made as described previously[6].

Western blot

PAVEC were grown to 70% confluency in a 75 cm^2 tissue culture flasks, then lysed directly on the plate using RIPA buffer supplemented with 25mM NaF, 1mM $NaVO_4$, and 0.5% Protease inhibitor cocktail (Sigma), incubated for 15 min at RT, scraped and homogenized by pipetting up and down, and centrifuged at 15,000 rpm for ten minutes. 10ug of protein was loaded into a 4–15% gradient gel (Bio-Rad, Hercules, CA) with 2× Laemmli buffer (Bio-Rad, Hercules, CA) at 1:1 ratio and run for one hour at 120V in 25mM Tris, 0.2M Glycine, 1% SDS running buffer. Western blot transfer to nitrocellulose membrane (Thermo Scientific, Rockford, IL) was performed at 400mA for one hour in 25mM Tris, 20% methanol transfer buffer. After rinsing in PBS 0.1% Tween-20, membrane was blocked for one hour in Odyssey Blocking Buffer (Li-Cor, Lincoln, NE) at RT. Mouse anti-human VE-cadherin (Abcam, Cambridge, MA) (1:1000), rabbit anti-human alpha-smooth muscle actin (Abcam, Cambridge, MA) (1:1000), and mouse antihuman GAPDH (Invitrogen, Grand Island, NY) (1:10,000) were used in Odyssey blocking buffer+0.1%Tween-20 to detect protein expression. The membrane was washed 4× in PBStween, 1× in PBS, and incubated overnight at 4°C with gentle agitation. The same washes were then performed and the membrane was incubated in Odyssey blocking buffer +0.1% Tween-20 +0.2% SDS with 1:20,000 anti-mouse and anti-goat secondary antibodies (Li-Cor IRDye, Lincoln, NE). Blots were imaged using the Odyssey Infrared system (Li-Cor, Lincoln, NE). After purity of endothelial population was confirmed, PAVEC from the same cell isolation were used in membrane system experiments.

Immunofluorescence

Intact membrane system (with cells on membrane and/or within collagen gel) was rinsed twice in PBS and fixed in 4% paraformaldehyde for one hour at 37°C. Samples were rinsed three times on a rocker with PBS for 15 minutes each, permeabilized with 0.2% Triton-X (VWR International, West Chester, PA) for ten minutes on rocker, and blocked in 10% goat serum for one hour at 37°C. Samples were rinsed briefly in PBS and primary antibodies were added: mouse anti-pig CD31 (AbD Serotec, Kidlington, UK, 1:100), rabbit anti-human αSMA (Abcam, Cambridge, MA, 1:100), rabbit anti-human Snai1 (Santa Cruz Biotechnoloy, Dallas, TX, 1:50) and AlexaFluor 488® phalloidin (Invitrogen, Grand Island, NY, 1:100). Samples were incubated overnight at 4°C, rinsed three times in PBS on rocker for 15 minutes each, and species-specific secondary antibodies raised in goat conjugated to

Alexa Fluor® 488 or 568 fluorophores were added (Invitrogen, Grand Island, NY 1:100). Samples were incubated for two hours at room temperature, rinsed, then incubated for an additional 30 minutes with Draq5 nuclear stain (Enzo Life Sciences AG, Lausen, Switzerland, 1:1000). Samples were rinsed thoroughly in PBS three times on rocker for 15 minutes each, then imaged using a Zeiss 710 (Thornwood, NY) laser scanning confocal microscope. Confocal reflectance was used to image collagen fibers within the gel, collected as a separate stack but with identical spatial-resolution settings as the immunofluorescence imaging.

Quantitative real-time polymerase chain reaction

To separately isolate PAVEC remaining on the membrane from PAVEC within the collagen gel, the collagen gel was first removed from the membrane system and vortexed in RLT buffer plus 1% beta-mercaptoethanol (Qiagen, Valencia, CA) until dissolved and frozen at −80°C. The membrane was then submerged in 0.25% trypsin-EDTA for five minutes at 37°C. Three times the volume of media was added to the membrane unit to stop the trypsin reaction and any remaining cells were scraped gently from the membrane. The cell, trypsin, and media solution was then spun down at 1000rpm for five minutes at room temperature. The cell pellet was rinsed in 1x PBS, resuspended in RLT buffer plus 1% beta-mercaptoethanol, and frozen at −80°C.

Total RNA was extracted using a RNeasy total RNA purification kit (Qiagen, Valencia, CA) and RNA was reverse transcribed to cDNA using the iScript™ cDNA synthesis kit (Biorad, Hercules, CA). Quantitative real-time PCR was performed on all samples using SYBR Green PCR master mix (Applied Biosystems, Foster City, CA), and a CFX96 or MiniOpticon Real-Time PCR Detection System (Bio-Rad, Hercules, CA) (Table 1).

Data analysis

All experiments were performed with $n \geq 3$. Data is expressed as mean ± standard error of the mean (SEM). All comparisons between two groups were made using two-tailed, unpaired t-tests assuming unequal variance. Comparisons between multiple groups were made using ANOVA. Differences between means were considered significant when $p < 0.05$.

Results

Culture system supports maintenance of PAVEC monolayers and collagen invasion

Pure populations of healthy PAVEC, with confirmed expression of VE-cadherin and no αSMA (Figure 2A), were cultured for up to six days on either the 3μm membrane (Figure 2B) or the 8μm membrane (Figure 2C). PAVEC cultured on membranes form confluent monolayers with strong CD31 expression and cobblestone morphology (Figure 2D). PAVEC have no αSMA expression and do not invade the underlying gel (Figure 2E,F). When treated with TNFα, a subset of PAVEC passes through the membrane and invades the underlying gel (Figure 2G).

We then used confocal microscopy to image PAVEC undergoing EndMT on the membrane system (Figure 3). Viewed from above, *en face* to the membrane surface, we observed heterogeneity in the expression of αSMA within PAVEC remaining on the membrane. All PAVEC expressed CD31 (red), but only a subset had increased αSMA expression (green, arrows) (Figure 3A). Using a three-dimensional reconstruction to view the system from the side, we imaged a single PAVEC passing through a membrane pore (Figure 3A, arrowheads; Figure 3B, dashed lines). The invading cell had increased αSMA (green) and decreased CD31 (red, arrow), consistent with an EndMT phenotypic shift. When the same cell field

was reconstructed as a three-dimensional image (Figure 3C), the same invading cell was seen to be protruding into the collagen gel (arrow). Other PAVEC were also observed to be invading the gel (asterisks). A subset of PAVEC remained on the surface of the membrane (Figure 3B, 3C). These cells were variably distributed across the membrane pores (Figure 3A), suggesting that proximity to a pore was not the primary factor in deciding whether a cell would invade. This variation in invasion suggested that the initial population of VEC possessed variation in ability or propensity to undergo EndMT with TNFα stimulus.

Time-dependent dynamics of TNFα-EndMT

Using the membrane system to separate transformed PAVEC (T-VEC) from non-transformed PAVEC (NT-VEC), we characterized the EndMT phenotype of both cell populations after two, four, or six days of TNFα treatment. All treatment groups (T-VEC and NT-VEC) were compared to PAVEC cultured on the membrane for equal lengths of time in control media. There was no invasion in control groups. Using the 3μm pore membrane, we found that endothelial cell-cell adhesion protein VE-cadherin was increased in NT-VEC at day two (2.08 ± 0.19 fold, p=0.01)) and remains similar to control levels through day four (0.68±0.1 fold, p=0.23) and day six (0.82±0.1 fold, p=0.32) (Figure 4A). The initial increase in VE-cadherin expression may be due to the re-organization of cell-cell contacts as subsets of PAVEC invade and NT-VEC form new attachments. The gene encoding transcription factor Snail (Snai1), which is associated with EMT[7], was increased in both NT-VEC (7.6±2.8 fold, p=0.008) and T-VEC (4.4±0.2 fold, p=0.05) after two days of treatment, when compared to PAVEC treated with control media (Figure 4B). At four days, Snai1 was decreased in NT-VEC (0.36±0.04 fold, p=0.09) and increased in T-VEC (7.81±1.5 fold, p=0.02). At six days, Snai1 was decreased in NT-VEC (0.13±0.01 fold) and increased in T-VEC (2.4±0.9 fold, p=0.02). NT-VEC maintained low expression of αSMA through day two (1.05±0.4, p=0.3), four (0.23±0.09, p=0.02), and six (not detectable). However, T-VEC increased in αSMA over time, through day two (3.1±1.0 fold, p=0.1), day four (2.13±0.2 fold, p=0.1), and day six (15.6±1.1 fold, p=0.006) (Figure 4C).

To understand the effects of pore size on the time dynamics of PAVEC TNFα-EndMT, we repeated the EndMT time-course experiments with an 8μm pore-size membrane. We found that the stages of EndMT were the same with the larger pores, but occurred more rapidly. NT-VEC had decreased VE-cadherin at day two (0.18±0.01 fold, p=0.0001) which could be due to reorganization of cell-cell contacts during the first phase of invasion. NT-VEC had VE-cadherin levels similar to control samples at day three (0.8±0.2 fold, p=0.3) and day four (0.8±0.06 fold, p=.07). T-VEC had increased expression of VE-cadherin at day three (5.0±1.9 fold, p=0.4), suggesting that transformed cells maintain some of their endothelial characteristics as they invade. T-VEC had decreased VE-cadherin by day four (0.1±0.1 fold, $p>10^{-6}$), indicating progressive mesenchymal transformation (Figure 4D). NT-VEC had levels of Snai1 lower than control at day two (0.5±0.02 fold, p=0.02), and similar to control at day three (2.0±0.5 fold, p=0.15) and day four (1.1±0.01 fold, p=0.3). Snai1 expression was increased in T-VEC at day three (22.5±3.2 fold, $p< 10^{-3}$) and returned to control levels by day four (Figure 5E). Absence of an upregulation in Snai1 in NT-VEC could be attributed to the larger pore size, which allows EndMT cells to undergo full mesenchymal transformation more rapidly. Thus, Snai1 increase may occur prior to the two-day time-point. NT-VEC had αSMA levels similar to control. T-VEC had low levels of αSMA at day two (0.01±0.003 fold, p=0.4) and day three (0.8±0.5 fold, p=0.03). T-VEC had increased αSMA at four days after treatment (14.8±2.5 fold, $p< 10^{-4}$), rather than the six days required for increased αSMA in the 3μm system (Figure 4F). These results suggest that a larger pore size does not affect the mechanism of progression of TNFα-EndMT in PAVEC, but allows the process to occur more rapidly.

EndMT protein expression in transforming valve endothelial cells

To confirm the changes in gene expression and time dynamics of EndMT observed in the membrane system, we analyzed expression and localization of CD31, Snail, and αSMA proteins in NT-VEC and T-VEC across two, four, and six days of treatment on the 3μm pore membrane. NT-VEC had initial increases in Snail expression and nuclear localization at day two, which was decreased at day four and six. NT-VEC consistently expressed membranous CD31, an endothelial marker (Figure 5A–C). T-VEC co-expressed CD31 and αSMA at day two, with increasing αSMA at day four and day six (Figure 5D–F). CD31 expression decreased at day six, but was still observable at some cell-cell junctions (Figure 5F, arrows).

Characterization of transformed valve endothelial cells

We then used the membrane system to characterize expression of genes related to valve disease in both NT-VEC and T-VEC. We compared NT-VEC and T-VEC with untreated VEC controls, with porcine aortic valve interstitial cells (VIC) embedded in the collagen gel with no treatment, and with embedded VIC treated with TNFα. Control VEC (0.05±0.02 fold, p=0.03) and NT-VEC (not detected) had very low levels of MMP-9 compared to control VIC. T-VEC, however, had very high levels of MMP-9 (250±43 fold, p=0.0002) compared to control VIC (Figure 6A). VIC+TNFα also had elevated MMP-9 (3.0±0.24 fold, p=0.043) compared to control VIC. TGF-β1 was increased in T-VEC (6.9±1.5 fold, p=0.009) and VIC+TNFα (6.1±1.0 fold, p=0.002) compared to control VIC (Figure 6B). Notch1 was increased in control VEC (3.78±0.24 fold, p=0.002), T-VEC (75.8±4.7 fold, p=0.003), and VIC+TNFα (4.1±0.4 fold, p=0.0009) compared to control VIC. NT-VEC (1.39±0.04 fold, p=0.09) had similar levels of Notch1 as control VIC (Figure 6C). BMP-4 was increased in control VEC (6.98±0.6 fold, p=0.002), T-VEC (38.84±0.4 fold, p=0.006), and VIC+TNFα (3.63±1.1 fold, p=0.05) compared to control VIC (Figure 6D). NT-VEC (0.78±0.13, p=0.34) had similar levels of BMP-4 as control VIC.

We also examined expression of inflammatory adhesion molecules ICAM-1 and VCAM-1 in all groups compared to control VEC. ICAM-1 was increased in NT-VEC (2.0±0.2 fold, p=0.009), T-VEC (5.05±1.9 fold, p=0.05), and VIC+TNFα (2.4±0.4 fold, p=0.004) compared to control VEC (Figure 6E). Control VIC had similar levels of ICAM-1 as control VEC (0.97±0.04 fold, p=0.79). VCAM-1 was increased in NT-VEC (1.6±0.1 fold, p=0.009) and VIC+TNFα (1.4±0.2 fold, p=0.047) compared to control VEC. Control VIC had similar levels of VCAM-1 as control VEC (1.1±0.12, p=0.49)(Figure 6F). Finally, we quantified levels of the gene encoding endothelial nitric oxide synthase (eNOS), NOS3, across groups compared to control VEC as a further examination of endothelial phenotype. NT-VEC had similar levels of NOS3 as control VEC (0.9±0.09 fold, p=0.42), while T-VEC (0.23±0.4, p=0.16), control VIC (0.09±0.01 fold, $p< 10^{-3}$), and VIC+TNFα (0.27±0.04 fold, $p=10^{-3}$) had decreased levels of NOS3 compared to control VEC (Figure 6G).

Transformed valve endothelial cells rearrange collagen extracellular matrix

Lastly, we further characterized the phenotype of T-VEC by assessing the arrangement of collagen fibers in gels containing T-VEC versus gels with control VEC or VIC. Control VEC cultured directly on collagen gels did not affect the arrangement of collagen fibers (Figure 7A). In contrast, collagen fibers in the region of T-VEC were elongated and aligned with the long axes of the transformed cells (Figure 7B, dashed double arrows). VIC embedded in an identical collagen gel did not affect collagen fiber alignment (Figure 7C). Similar to the control VEC condition, the fibers in the VIC gels were short and randomly oriented. The ability of T-VEC to interact with the collagen gel suggests that T-VEC may be able to play a role in affecting the changes in extracellular matrix seen in AVD[10].

Discussion

A greater understanding of the heterogeneity, time-dependence and pathogenic role of valve endothelial cells undergoing mesenchymal transformation is necessary to connect EndMT pathophysiology with the treatment of aortic valve disease. Here we have utilized a novel *in vitro* system to characterize TNFα-induced EndMT in aortic valve endothelial cells. We identified a population of non-transforming aortic valve endothelial cells that resists TNFα - EndMT and retains an endothelial phenotype, and a population of transformed cells that acquires a mesenchymal and pro-disease phenotype with TNFα treatment.

Previous studies have employed clonal isolation systems to study and assess the ability of certain subgroups of VEC to undergo EndMT[3,4,26,32,33]. The use of primary cells cultured together on the membrane system described here is advantageous because it allows cell-cell communication between transforming and non-transforming cells, as would occur *in vivo*. Additionally, it is possible to separate transforming from non-transforming cells, post-EndMT. The advantages of the cell-cell communication allowed in this system can be expanded by using a location-specific isolation of VEC such as those near the valve commissures which have shown increased inflammation in early disease[1], or a side-specific isolation. These further studies would capitalize on the ability to culture a heterogeneous population of cells while narrowing the window of examination.

The three-dimensional nature of this system has the advantage of allowing a more physiological mesenchymal transformation than traditional two-dimensional EndMT assays. An endothelial cell which has undergone full mesenchymal transformation will not only change morphology and phenotype, but will invade its underlying substrate and develop complex mechanisms of interaction with its three-dimensional extracellular environment[22]. This system allows full invasion of VEC undergoing EndMT into a more physiological environment of collagen hydrogel. Allowing matrix invasion makes assessment of traits such as matrix interactions and matrix metalloproteinase expression in transformed and non-transformed VEC possible. The results of this study suggest that VEC cultured on the membrane undergoing TNFα-stimulated EndMT invade the matrix to the same extent as VEC cultured directly on the hydrogel[24] (data not shown), despite the difference in stiffness between each surface. An assessment of the effect of the difference in stiffness between membrane and hydrogel could be easily conducted using membranes of different materials with different mechanical properties. The membrane used here can be adjusted via modulation of pore size, hydrogel composition, and membrane coating substrate.

Beyond developing a system for assessment of transforming and non-transforming VEC undergoing EndMT, we have evaluated the dynamics of this process in the initial response of VEC to TNFα. Our results show that inflammatory EndMT is a complex phenomenon with the potential to contribute to various elements of early valve disease. Mesenchymal transformation could contribute to a fraction of the endothelial denudation observed in diseased valves, linking inflammatory activation of the endothelium[17] to endothelial loss during the calcification stage[15]. Unraveling the time dynamics of EndMT in the valve is key in understanding the role of certain biological actors known to play complex parts in the progression of valve disease. For example, TGF-β is known to have both protective[23] and detrimental effects[31] in the aortic valve. These complex and seemingly opposing responses can be elucidated via this membrane system, which separates VEC as they transform or resist transformation, elucidating the time-dependency of each event. Further complexity could be assessed via addition of co-cultured valvular interstitial cells to the hydrogel component. Finally, the system can be used to screen anti-EndMT therapies (such as in the context of cancer or fibrosis)[11,19] in a stage-dependent manner.

The fate of adult VEC undergoing EndMT is unclear. This study provides initial evidence that TVEC may be participants in some of the early mechanisms of AVD, through increased expression of MMP-9, TGF-β1, Notch1, and BMP4, as well as via collagen remodeling. MMP-9 is expressed in stenotic but not healthy aortic valves[9], linking increased MMP-9 and T-VEC collagen remodeling to the changes in extracellular matrix organization observed in early valve disease. We note that remodeling of a collagen hydrogel is not the same as T-VEC affecting the complex ECM composition of a native valve, but their aggressive invasive phenotype and distinct effects on collagen fiber alignment suggest that they have increased ability to affect their extracellular environment. TGF-β1 is known to be regulated by TNFα and is implicated in accelerating calcification of aortic valve interstitial cells[21,25]. T-VEC in this study had increased TGF-β1 mRNA, whereas NT-VEC had levels comparable to quiescent VIC. T-VEC may contribute to levels of TGF-β1 in the diseased aortic valve, accelerating calcification of native VIC. Notch1 initiates EndMT in the developing valve[8] and in postnatal aortic VEC[33]. Notch1 was increased in T-VEC, agreeing with a link to valve EndMT. Interestingly, levels of Notch1 in NT-VEC were comparable to VIC controls and lower than control VEC, suggesting that they may have a decreased EndMT potential or a native predisposition against EndMT. Future studies are needed to assess whether Notch1 levels in T-VEC could be repressed over longer timescales, as has been shown in animal models of aortic valve calcification. BMP-4 mediates endothelial inflammatory activation[30], promotes vascular calcification[5], and initiates EndMT in valvulogenesis[20]. BMP4 antagonists are repressed in CAVD[2]. BMP-4 was decreased in NTVEC, agreeing with a quiescent or protective role for these cells in valve disease. BMP-4 was increased in T-VEC, which could contribute both to a continued EndMT-activation paradigm and to acceleration of calcification. Sustained activation of inflammatory adhesion molecules ICAM-1 and VCAM-1 in NT-VEC suggests that the population of VEC that resists transformation under TNFα treatment is able to maintain an inflammatory phenotype while not undergoing an EndMT response. This result, coupled with the sustained endothelial phenotype of these cells as evidenced by maintaining control levels of VE-cadherin and endothelial nitric oxide synthase, suggest that this population of cells may possess a distinct molecular signature which protects against some of the detrimental effects of inflammation.

This study is an initial investigation of the differences in aortic valve endothelial response to TNFα, specifically regarding the EndMT response mechanism. The *in vitro* nature of the study makes it well suited for separating distinct cell populations and characterizing their time-dependent response to treatment. We recognize that TNFα treatment represents one facet of early aortic valve disease and the EndMT response is a single component of a complex pathological phenomenon. In addition, our method of harvesting cells from across the entire surface of the porcine aortic valve, rather than in a side-specific manner, does offer continuing avenues of exploration in terms of identifying whether transforming VEC come preferentially from certain regions of the aortic valve surface or whether tendency to transform is effected from extracellular phenomenon such as shear stress or strain. These elements could easily be incorporated into the system described in this study, with the same benefits of ability to separate distinct populations and allow fully three-dimensional invasion and matrix interactions. Overall, the three-dimensional nature of the system, the molecular signatures identified between transforming and non-transforming populations, and the amenability of the technique to increasing levels of complexity across time, cell type, and endpoint analysis lays an important foundation for understanding the role of EndMT in valve disease progression.

Conclusion

In the present study, we have designed a system that allows for highly specified characterization of EndMT dynamics. We have built upon previous studies to validate the ability of the system to allow healthy endothelial cells treated with TNFα to undergo the full phenotypic shift characteristic of EndMT, including repression of endothelial proteins, upregulation of mesenchymal proteins, and invasion into a three-dimensional collagen hydrogel environment. We have shown that the subset of VEC which undergo TNFα-EndMT may have unique abilities to contribute to the earliest stages of AVD via collagen remodeling and increased MMP-9, TGF-β1, Notch1, and BMP-4 expression. The subset of VEC which resists TNFα-EndMT is shown to express inflammatory adhesion proteins, yet retain endothelial characteristics such as VE-cadherin, CD31, and endothelial nitric oxide synthase expression. The results of this study provide an important baseline for isolation and characterization of VEC, which have undergone postnatal EndMT. We have shown for the first time that transformed valve endothelial cells have a phenotype which suggests they could contribute to advanced AVD, that there exists a subpopulation of valve endothelial cells with resistance to TNFα-EndMT, and designed a system which can be used for investigation of EndMT dynamics across physiological contexts.

Acknowledgments

The authors would like to thank Shirks Meats of Dundee, NY for providing porcine aortic valves. This study was supported by the National Science Foundation Graduate Research Fellowship (EF), the Alfred P. Sloan Foundation (EF), NIH grant HL110328, NSF CBET-0955172, and the LeDucq Foundation.

References

1. Aikawa E, Nahrendorf M, Sosnovik D, Lok VM, Jaffer FA, Aikawa M, Weissleder R. Multimodality molecular imaging identifies proteolytic and osteogenic activities in early aortic valve disease. Circulation. 2007; 115:377–386. [PubMed: 17224478]
2. Ankeny RF, Thourani VH, Weiss D, Vega JD, Taylor WR, Nerem RM, Jo H. Preferential activation of SMAD1/5/8 on the fibrosa endothelium in calcified human aortic valves: association with low BMP antagonists and SMAD6. PLoS ONE. 2011; 6:e20969. [PubMed: 21698246]
3. Balachandran K, Alford P, Wylie-Sears J, Goss JA, Grosberg A, Bischoff J, Aikawa E, Levine RA, Parker KK. Cyclic strain induces dual-mode endothelial-mesenchymal transformation of the cardiac valve. Proc. Natl. Acad. Sci. U. S. A. 2011:19943–19948. [PubMed: 22123981]
4. Bischoff J, Aikawa E. Progenitor cells confer plasticity to cardiac valve endothelium. J. of Cardiovasc. Trans. Res. 2011; 4:710–719.
5. Boström K, Watson KE, Horn S, Wortham C, Herman IM, Demer LL. Bone morphogenetic protein expression in human atherosclerotic lesions. J. Clin. Invest. 1993; 91:1800–1809. [PubMed: 8473518]
6. Butcher JT, Nerem RM. Valvular endothelial cells regulate the phenotype of interstitial cells in co-culture: Effects of steady shear stress. Tissue Eng. 2006; 12:905–915. [PubMed: 16674302]
7. Cano A, Pérez-Moreno MA, Rodrigo I, Locascio A, Blanco MJ, del Barrio MG, Portillo F, Nieto MA. The transcription factor Snail controls epithelial–mesenchymal transitions by repressing E-cadherin expression. Nat. Cell. Biol. 2000; 2:76–83. [PubMed: 10655586]
8. Chang ACY, Fu Y, Garside VC, Niessen K, Chang L, Fuller M, Setiadi A, Smrz J, Kyle A, Minchinton A, Marra M, Hoodless PA, Karsan A. Notch initiates the endothelial-to-mesenchymal transition in the atrioventricular canal through autocrine activation of soluble guanylyl cyclase. Dev. Cell. 2011; 21:288–300. [PubMed: 21839921]
9. Edep ME, Shirani J, Wolf P, Brown DL. Matrix metalloproteinase expression in nonrheumatic aortic stenosis. Cardiovasc. Pathol. 2000; 9:281–286. [PubMed: 11064275]
10. Fondard O, Detaint D, Lung B, Choqueux C, Adle-Biassette H, Jarraya M, Hvass U, Couetil JP, Henin D, Michel JB, Vahanian A, Jacob MP. Extracellular matrix remodeling in human aortic

valve disease: The role of matrix metalloproteinases and their tissue inhibitors. Eur. Heart J. 2005; 26:1333–1341. [PubMed: 15827062]

11. Galichon P, Hertig A. Epithelial to mesenchymal transition as a biomarker in renal fibrosis: are we ready for the bedside? Fibrog. Tissue Repair. 2011; 4:11.
12. Garg V, Muth AN, Ransom JF, Schluterman MK, Barnes R, King IN, Grossfeld PD, Srivastava D. Mutations in NOTCH1 Cause Aortic Valve Disease. Nature. 2005; 437:270–274. [PubMed: 16025100]
13. Ghaisas N, Foley J, O'Briain D, Crean P, Kelleher D, Walsh M. Adhesion molecules in nonrheumatic aortic valve disease: Endothelial expression, serum levels and effects of valve replacement. J. Am. Coll. Cardiol. 2000; 36:2257–2262. [PubMed: 11127470]
14. Go AS, et al. Heart disease and stroke statistics--2013 Update: A report from the American Heart Association. Circulation. 2013; 127:e6–e245. [PubMed: 23239837]
15. Goldbarg SH, Elmariah S, Miller MA, Fuster V. Insights into degenerative aortic valve disease. J. Am. Coll. Cardiol. 2007; 50:1205–1230. [PubMed: 17888836]
16. Gould RA, Butcher JT. Isolation of Valvular Endothelial Cells. J. Visualized Exp. 2010; 46:1–5.
17. Guerraty MA, Grant GR, Karanian JW, Chiesa OA, Pritchard WF, Davies PF. Hypercholesterolemia induces side-specific phenotypic changes and peroxisome proliferator-activated receptor- pathway activation in swine aortic valve endothelium. Arterioscler., Thromb., Vasc. Biol. 2010; 30:225–231. [PubMed: 19926833]
18. Hjortnaes J, Butcher J, Figueiredo JL, Riccio M, Kohler RH, Kozloff KM, Weissleder R, Aikawa E. Arterial and aortic valve calcification inversely correlates with osteoporotic bone remodelling: a role for inflammation. Eur. Heart J. 2010; 31:1975–1984. [PubMed: 20601388]
19. Hollier BG, Tinnirello AA, Werden SJ, Evans KW, Taube JH, Sarkar TR, Sphyris N, Shariati M, Kumar SV, Battula VL, Herschkowitz JI, Guerra R, Chang JT, Miura N, Rosen JM, Mani SA. FOXC2 expression links epithelial-mesenchymal transition and stem cell properties in breast cancer. Cancer Res. 2013; 73:1981–1992. [PubMed: 23378344]
20. Jia Q, McDill BW, Li S-Z, Deng C, Chang C-P, Chen F. Smad signaling in the neural crest regulates cardiac outflow tract remodeling through cell autonomous and noncell autonomous effects. Dev. Biol. 2007; 311:172–184. [PubMed: 17916348]
21. Jian B, Narula N, Li Q, Mohler E, Levy R. Progression of aortic valve stenosis: TGF-beta 1 is present in calcified aortic valve cusps and promotes aortic valve interstitial cell calcification via apoptosis. Ann. Thorac. Surg. 2003; 75:457–465. [PubMed: 12607654]
22. Kalluri R, Weinberg RA. The basics of epithelial-mesenchymal transition. The Journal of Clinical Investigation. 2009; 119:1420–1428. [PubMed: 19487818]
23. Liu AC, Gotlieb AI. Transforming growth factor-β regulates in vitro heart valve repair by activated valve interstitial cells. Am. J. Pathol. 2008; 173:1275–1285. [PubMed: 18832581]
24. Mahler GJ, Farrar EJ, Butcher JT. Inflammatory Cytokines Promote Mesenchymal Transformation in Embryonic and Adult Valve Endothelial Cells. Arterioscler., Thromb., Vasc. Biol. 2013; 33:121–130. [PubMed: 23104848]
25. Mohler ER, MK C, AW C, N V, RJ L, L G, FH G. Identification and characterization of calcifying valve cells from human and canine aortic valves. J. Heart Valve Dis. 1999; 8:254–260. [PubMed: 10399657]
26. Paranya G, Vineberg S, Dvorin E, Kaushal S, Roth SJ, Rabkin E, Schoen FJ, Bischoff J. Aortic valve endothelial cells undergo transforming growth factor-beta-mediated and non-transforming growth factor-beta-mediated transdifferentiation in vitro. Am. J. Pathol. 2001; 159:1335–1343. [PubMed: 11583961]
27. Richards J, El-Hamamsy I, Chen S, Sarang Z, Sarathchandra P, Yacoub MH, Chester AH, Butcher JT. Side-specific endothelial-dependent regulation of aortic valve calcification: Interplay of hemodynamics and nitric oxide signaling. Am. J. Pathol. 2013; 182:1922–1931. [PubMed: 23499458]
28. Simmons CA, Grant GR, Manduchi E, Davies PF. Spatial heterogeneity of endothelial phenotypes correlates with side-specific vulnerability to calcification in normal porcine aortic valves. Circulation Res. 2005; 96:792–799. [PubMed: 15761200]

29. Stewart, WJ.; Carabello, BA. Aortic Valve Disease. In: Topol, EJ.; Califf, RM.; Prystowsky, EN.; Thomas, JD.; Thompson, PD., editors. Textbook of Cardiovascular Medicine. Philadelphia, PA: Lippincott Williams, & Wilkins; 2006. p. 366p. 388

30. Sucosky P, Balachandran K, Elhammali A, Jo H, Yoganathan AP. Altered shear stress stimulates upregulation of endothelial vcam-1 and icam-1 in a bmp-4–and tgf-β1–dependent pathway. Arterioscler., Thromb., Vasc. Biol. 2009; 29:254–260. [PubMed: 19023092]

31. Walker GA, Masters KS, Shah DN, Anseth KS, Leinwand LA. Valvular myofibroblast activation by transforming growth factor-beta: Implications for pathological extracellular matrix remodeling in heart valve disease. Circulation Res. 2004; 95:253–260. [PubMed: 15217906]

32. Wylie-Sears J, Aikawa E, Levine RA, Yang J-H, Bischoff J. Mitral valve endothelial cells with osteogenic differentiation potential. Arterioscler., Thromb., Vasc. Biol. 2011; 31:598–607. [PubMed: 21164078]

33. Yang J-H, Wylie-Sears J, Bischoff J. Opposing actions of Notch1 and VEGF in post-natal cardiac valve endothelial cells. Biochem. Biophys. Res. Commun. 2008; 374:512–516. [PubMed: 18647596]

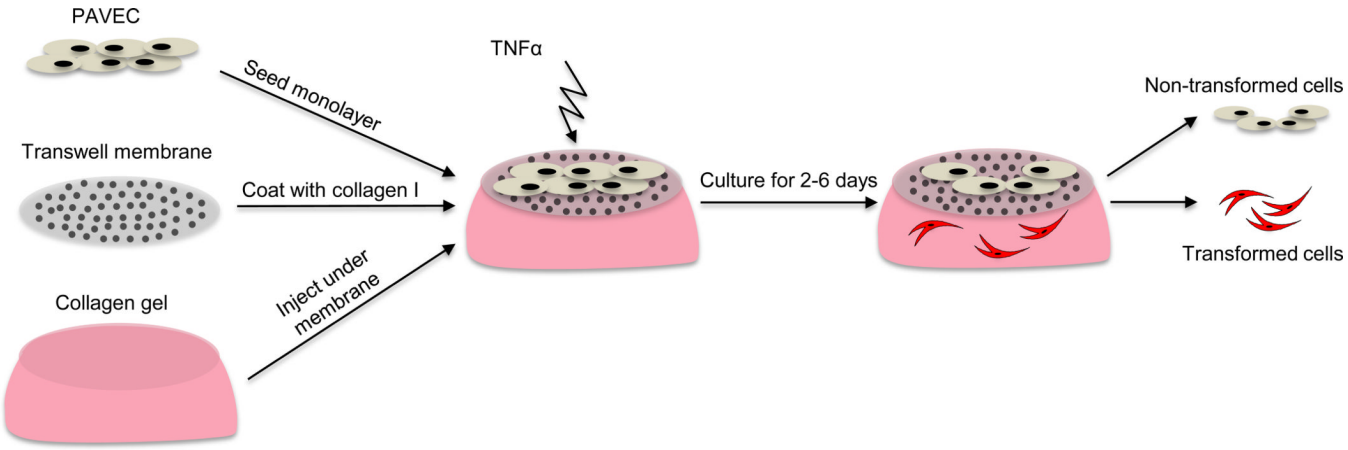

Figure 1.
Membrane-based platform for culture of endothelial cells and evaluation of EndMT response. PAVEC are cultured on a porous membrane which rests on a type I collagen hydrogel. PAVEC are exposed to TNFα treatment for 2–6 days. A subset of PAVEC undergo an endothelial to mesenchymal transformation and a subset remains on the membrane. Cells remaining on membrane are harvested separately from cells that have migrated into the gel.

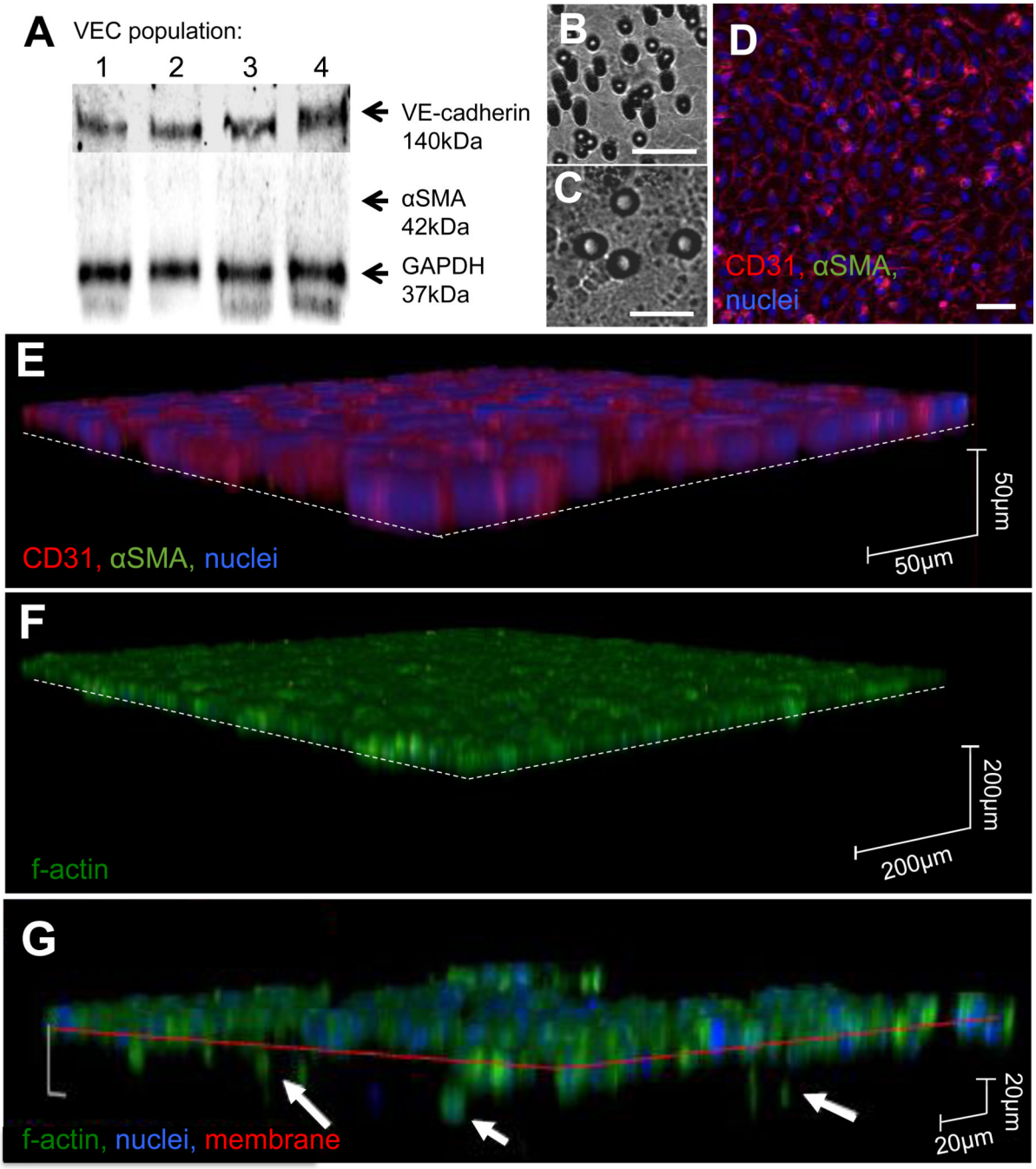

Figure 2.

Characterization of membrane culture system and EndMT response to TNFα. A. Western blot analysis of a random sampling of four of the populations of PAVEC used in the study. Populations of PAVEC were sampled for western blot analysis of protein content at passage three and used in experiments at passages four to six. All populations showed strong VE-cadherin expression and no αSMA expression. B, C. 3μm and 8μm membrane pores, scale bar is 20μm. D. PAVEC cultured on the membrane system for six days retain strong CD31 expression, no αSMA expression, and cobblestone morphology. Scale bar is 20μm. E, F. PAVEC cultured on the membrane system in control conditions for six days do not express αSMA and do not pass through the membrane into the hydrogel. G. After 48 hours of TNFα

treatment, a subset of PAVEC invade through the membrane into the hydrogel (arrows) and a subset remains on the membrane.

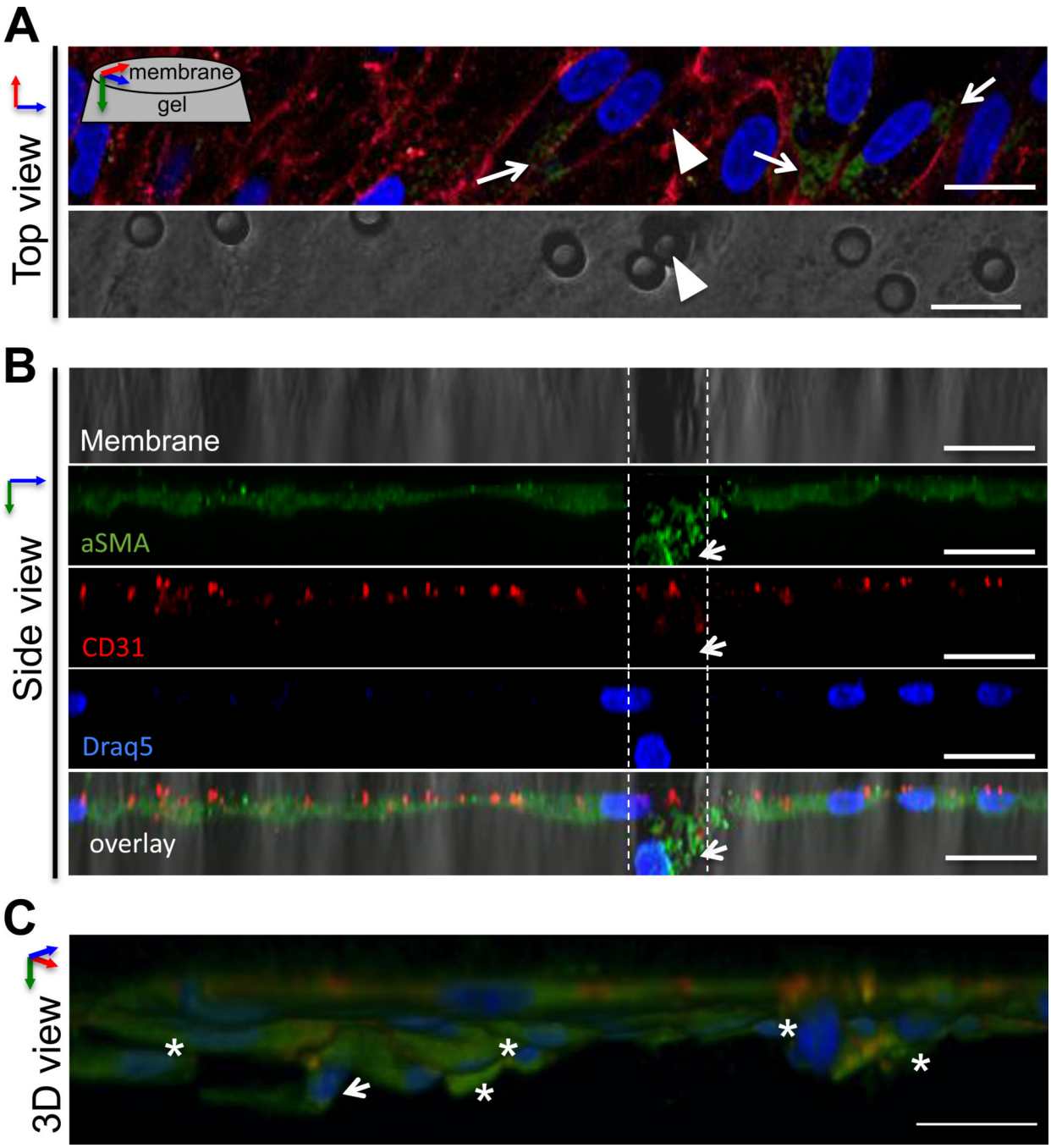

Figure 3.

Imaging of TNFα-EndMT process. A. Top view. After 48 hours of TNFα treatment, a subset of VEC have increased αSMA expression (arrows). In this image, a single VEC has begun to pass through a pore in the membrane (arrowhead). Lower panel shows 3μm membrane, arrowhead indicates the pore associated with the invading VEC. B. Side view of same cell field. Reconstruction of a high-resolution image stack of the same cell field as in A shows invasion of VEC through the pore (dashed lines). The migrating VEC has reduced CD31 and increased αSMA (arrow). C. Three-dimensional reconstruction of the same cell field as in A, B shows the same invading VEC (arrow), as well as other VEC in the same

region invading through the membrane into the hydrogel (asterisks). The invading cells have increased αSMA and express CD31. Scale bar is 20μm.

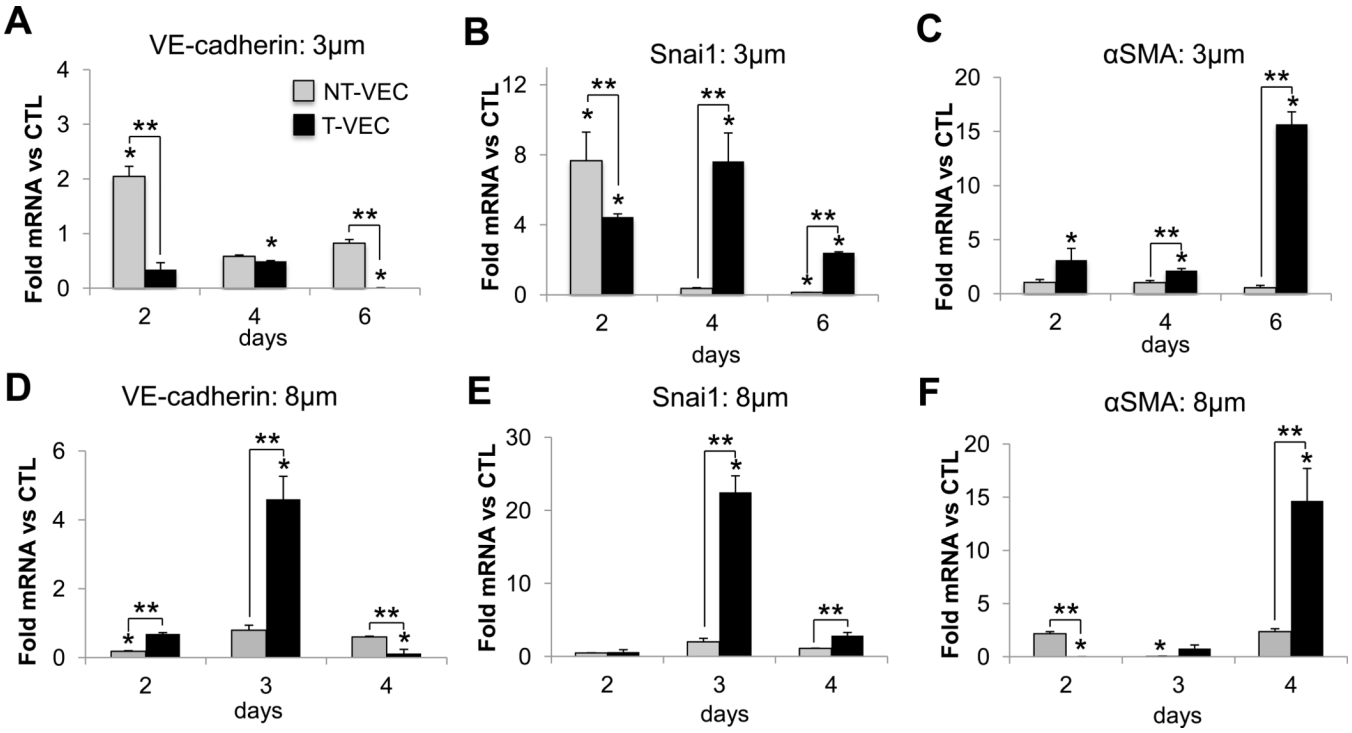

Figure 4.

Time-dependent expression of EndMT genes in VEC treated with TNFα. A–C, 3μm pore membrane. A. VE-cadherin expression was initially increased in NT-VEC and returned to control levels at day four and six. VE-cadherin decreased in the T-VEC population over time. B. Snai1 expression was elevated initially in both VEC populations. At day four, Snai1 decreased in NT-VEC to less than control and remained elevated in T-VEC until day six. C. αSMA expression was low in NT-VEC and increased in T-VEC. D–F, 8μm pore membrane. D. VE-cadherin expression was decreased in VEC remaining on membrane. Transformed VEC had elevated VE-cadherin expression on day three of treatment that is decreased by day four. E. Transformed VEC had elevated Snai1 expression after three days of treatment. F. Transformed VEC had highly elevated αSMA expression after four days of TNFα treatment. VEC remaining on membrane maintained αSMA levels similar to control (> 37 cycles). All experiments performed with n > 3. Errors bars indicate SEM. * indicates $p < 0.05$ versus control VEC at same time point; ** indicates $p < 0.05$ versus indicated group, according to ANOVA followed by Student's t-test.

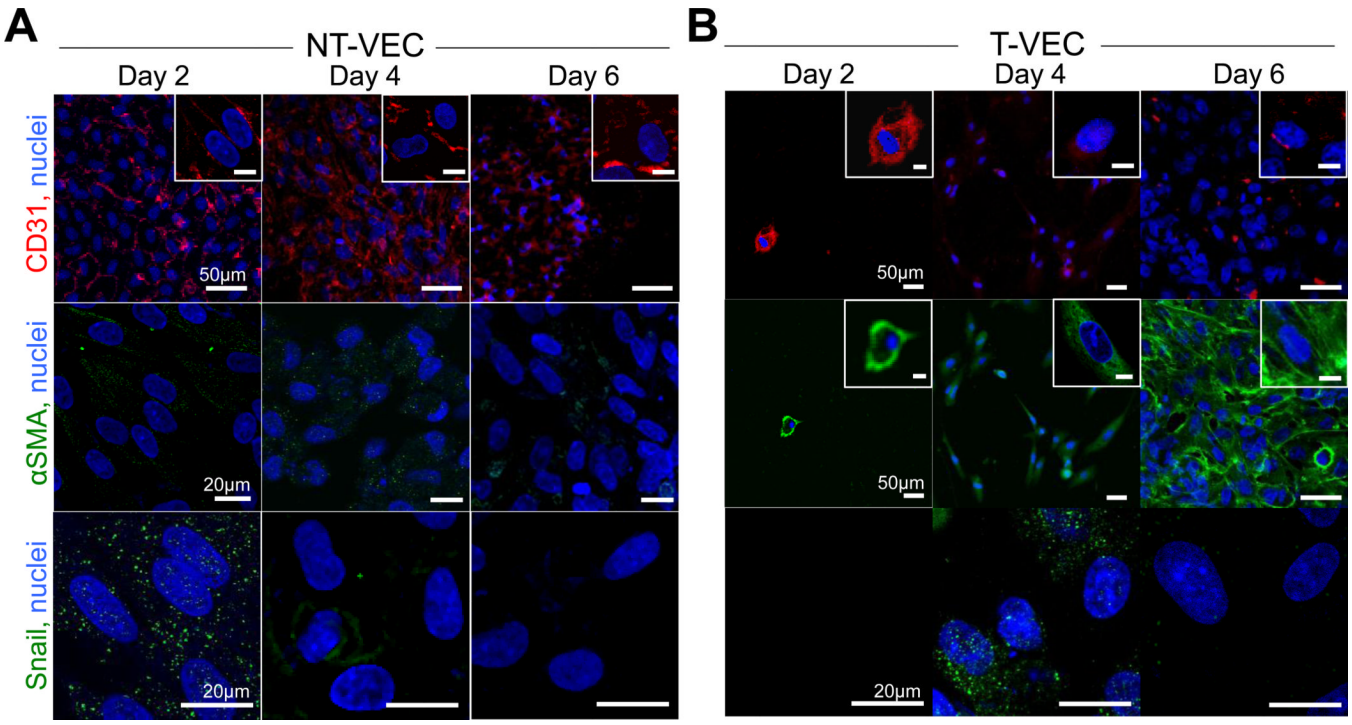

Figure 5.

Expression of EndMT proteins in non-transformed and transformed cells. A. CD31, Snail, and αSMA expression in non-transformed VEC (NT-VEC) after 2, 4, and 6 days of TNFα treatment. B. CD31, Snail, and αSMA expression in transformed VEC (T-VEC) after 2, 4, and 6 days of TNFα treatment. Images are representative of > 3 independent experiments. Scale bar length is indicated in leftmost panel of each row. Scale bar of inset images is 10μm.

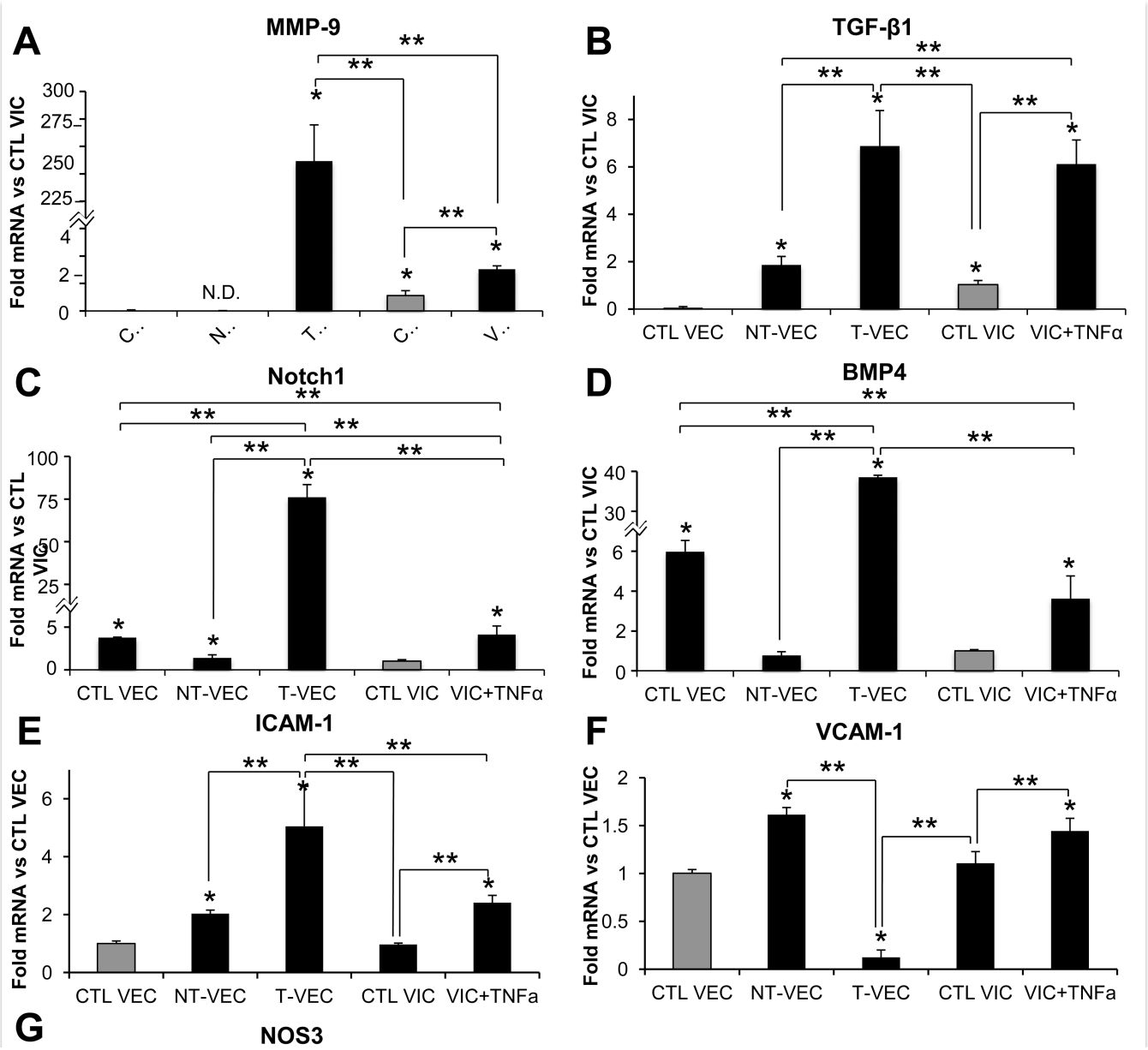

Figure 6.

Comparison of genes related to aortic valve pathogenesis in transformed and nontransformed VEC. A–D. All samples normalized to control VIC, isolated from membrane system or VIC hydrogels after two days of treatment. A. MMP-9 was elevated in T-VEC and VIC+TNFα but not in control VEC or NT-VEC. B. TGF-β1 was elevated in T-VEC and VIC+TNFα, at control levels in NT-VEC and decreased in control VEC, compared to control VIC. C. Notch1 was higher in control VEC, T-VEC, and VIC+TNFα compared to control VIC. NT-VEC had Notch1 levels similar to control VIC. D. BMP4 expression was higher in control VEC, T-VEC, and VIC+TNFα than in control VIC. NT-VEC had BMP4 levels similar to control VIC. E-G. All samples normalized to control VEC, isolated from membrane system or VIC hydrogel after two days of treatment. E. ICAM-1 levels were similar in control VEC and control VIC. NT-VEC, T-VEC, and VIC+TNFα had elevated ICAM-1 levels, with T-VEC having the highest expression. F. VCAM-1 levels

were similar in control VEC and control VIC. NT-VEC and VIC+TNFα had elevated VCAM-1 levels and T-VEC had decreased VCAM-1 compared to control VEC. G. NOS3 levels were similar in control VEC and NT-VEC. NOS3 levels were lower in T-VEC, control VIC, and VIC+TNFα compared to control VEC. All experiments performed with n > 3. Errors bars indicate SEM. * indicates $p < 0.05$ versus control; ** indicates $p < 0.05$ versus indicated group, according to ANOVA followed by Student's t-test. VCAM-1 indicates vascular cell adhesion protein 1; ICAM-1, intercellular adhesion molecule 1.

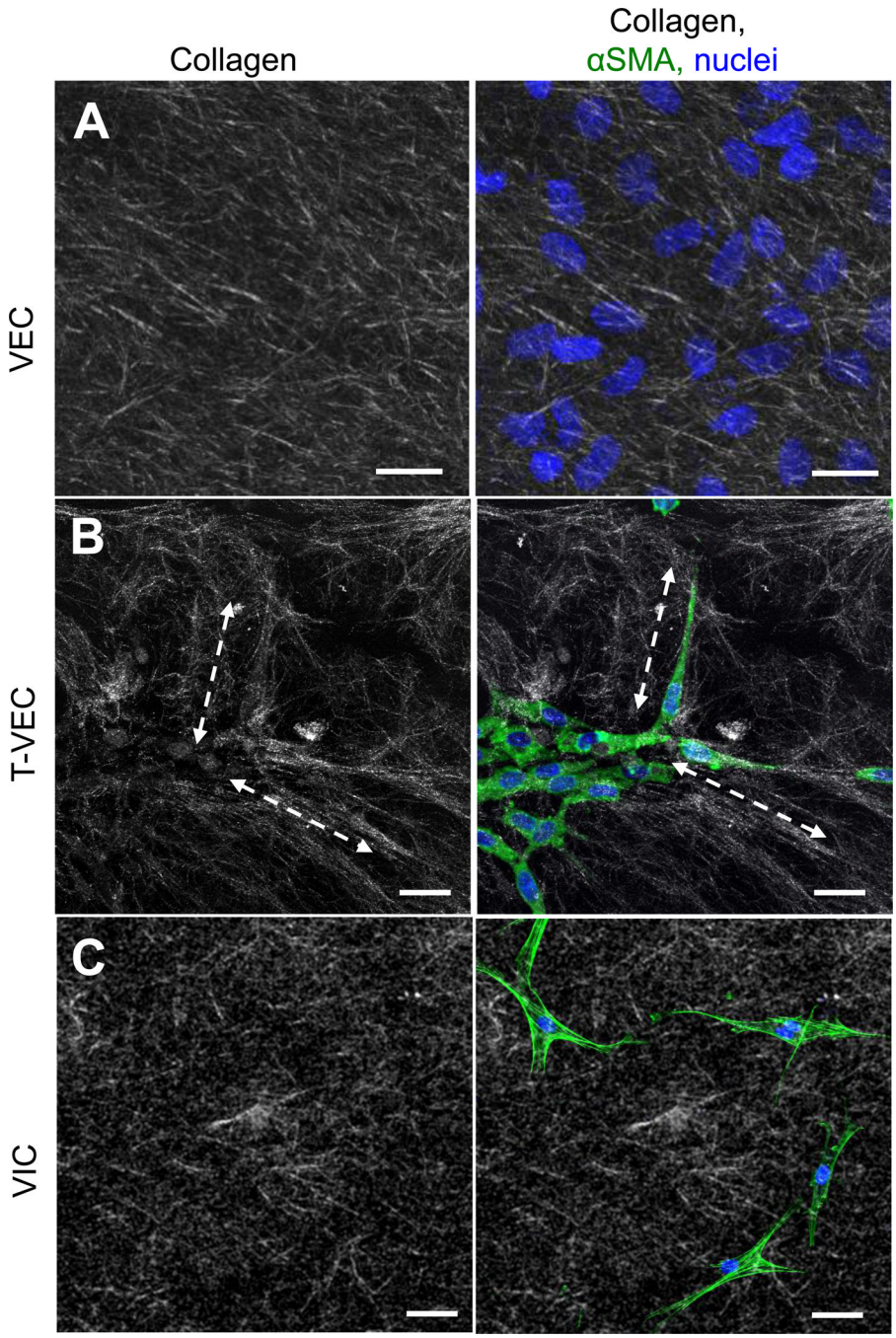

Figure 7.

Collagen fiber morphology and arrangement by transformed and non-transformed VEC. A. Collagen fibers in control gels (left panel) have random alignment and length. Control VEC seeded on the surface of a control gel did not change the alignment of collagen fibers (right). B. Collagen gels with invaded T-VEC, isolated as a whole gel from the membrane system and fixed immediately, had long collagen fibers (dashed lines) which were aligned with the long axis of T-VEC. C. Collagen gels with embedded valve interstitial cells had random alignment and length (left), not aligned with embedded VIC (right). Green = f-actin; representative images of n=4 experiments.

Table 1

Primer sequences for real-time quantitative polymerase chain reaction analysis of mRNA expression in porcine aortic valve endothelial and interstitial cells.

Gene	Forward primer	Reverse primer
18S	TAGAGGGACAAGTGGCGT	AATGGGGTTCAACGGGTT
ACTA2	CAGCCAGGATGTGTGAAGAA	TCACCCCCTGATGTCTAGGA
CD31	ATCTGCATCTCGTGGGAAGT	GAGCTGAAGTGTCAGCAGGA
Snai1	GCCCAACTACAGCGAGCTAC	CCAGGAGAGACTCCCAGATG
VE-cadherin	CGTGGTGGAAACACAAGATG	TGTGTACCTGGTCTGGGTGA
MMP-9	TGGGAGTACTGGCGACTCT	ACTTGGCGTCCAGAGAAGAA
TGF-b1	TTTCTGGTGGGGAGACAGAC	CTCCCCTAGGCTGCTTTCTT
Notch1	TGGATGGCATCAATTCCTTT	GGGCAGGTACACTTGTAGGC
BMP-4	AAAAAGTCGCCGAGATTCAG	CCGCATGTAATCTGGGATG
ICAM-1	AAAGGAGGCTCCATGAAGGT	TGCCATCGTTTTCCACATTA
VCAM-1	TTGTTGCCTCGTCACACAGC	CAATCTGCGCAATCATTTTG
NOS3	TGCATGACATTGAGAGCAAAGG	GATGGTCGAGTTGGGAGCAT